Supplemental Information

The affect of Aβ(39-42) on Aβ Aggregation

As demonstrated in the main text, Aβ42 only formed dimers through hexamers in our experiments in the presence of Aβ(39-42). For a qualitative assessment of the features in the ATD of z/n= -5/2, an injection energy study was performed. In an injection energy study, ions stored in the ion funnel are pulsed into the drift cell with a voltage, V. The translational energy given to the molecules is transferred through collisions with the Helium gas inside the drift cell leading first to internal excitation followed by thermalization. At high injection voltages, large noncovalent complexes, if present, may dissociate into small subunits. Figure S1 shows the ATD of z/n = -5/2 of a 5:1 Aβ(39-42):Aβ42 mixture. At 40 V, three features are present at 600, 640, and 690 μs (Figure S1a). As the injection energy is increased to 100V, the distribution shifts: the feature at 600 μs is diminished substantially and the feature at 690 μs dominates (Figure S1b). As no other features appear at longer times, the feature at 690 us may be assigned as the z = -5 dimer. Higher order oligomers with the same value of z/n always appear at shorter arrival times, allowing the feature at 600 μs to be assigned as the z = -15 hexamer and the feature at 640 μs as the z = -10 tetramer. No other peaks appear at shorter arrival times, indicating that under the conditions of our experiment, the largest oligomer observed is the hexamer.

The Aβ:CTF mixtures were held at 30°C for up to three weeks and reanalyzed using IM-MS. Figure S2 shows the ATD of z/n= -5/2 in a 1:5 mixture at t = 0 (a) and t = 21 d (b). The overall signal is significantly lower in (b), suggesting that the sample has aggregated. Large aggregates often clog the nano-ESI tips used in these experiments, lowering or even eliminating the analyte signal. Furthermore, as Aβ aggregates, the concentration of small oligomers in solution decreases, likely contributing to the low signal shown in this ATD. Still, similar features are visible in both ATDs, indicating that Aβ42 does not form decamer and dodecamer in the presence of 5-fold excess Aβ(39-42), even once larger aggregates have formed.

Similar experiments were performed with a 1:1 Aβ42:Aβ(39-42) mixture. The ATD of z/n= -5/2 of the mixture contains the same features as that of Aβ42 in the absence of inhibitor (Figure S3). This result indicates that one equivalent of Aβ(39–42) is not sufficient to modulate the assembly of Aβ42.

An arrival time distribution was also recorded for the peak at m/z = 1810 in Figure 5 of the main text, which represents an $n[2A\beta42 + A\beta(39\text{-}42)]^{-5n}$ species (Figure S4). Two features are present with cross sections that, although slightly larger than those of Aβ40 alone, closely correspond to a dimer and a tetramer of Aβ40 (1327 $Å^2$ and 2205 $Å^2$ respectively). This result indicates that the CTF binds to both dimers and tetramers of Aβ40.

Figure S1 An injection energy study of z/n=-5/2 of a 1:5 mixture of Aβ42 and Aβ(39-42). ATDs are shown at injection voltages of 40 V (a) and 100 V (b).

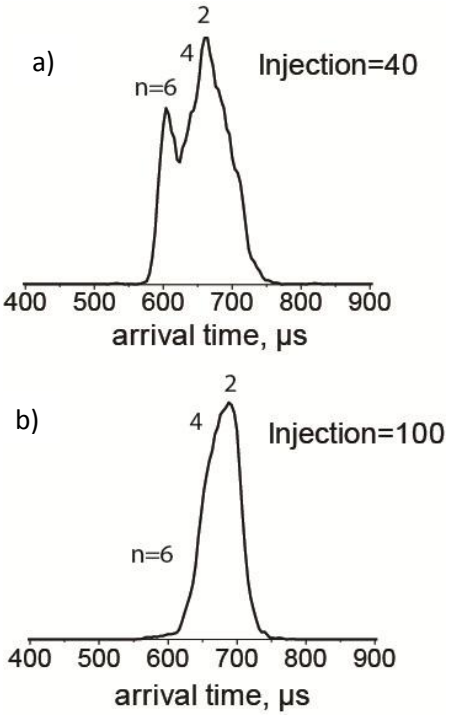

Figure S2 ATD of z/n=-5/2 of a 1:5 mixture of Aβ42 and Aβ(39-42) over time.

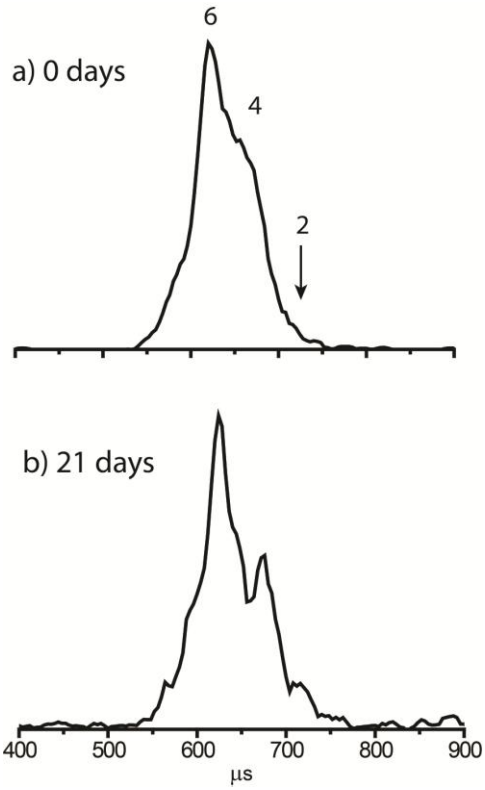

Figure S3 ATD of z/n=-5/2 of Aβ42 (a) and a 1:1 mixture of Aβ42 and Aβ(39-42) (b). Features corresponding to the dimer through dodecamer are present (n=12, 10, 6, 4, 2).

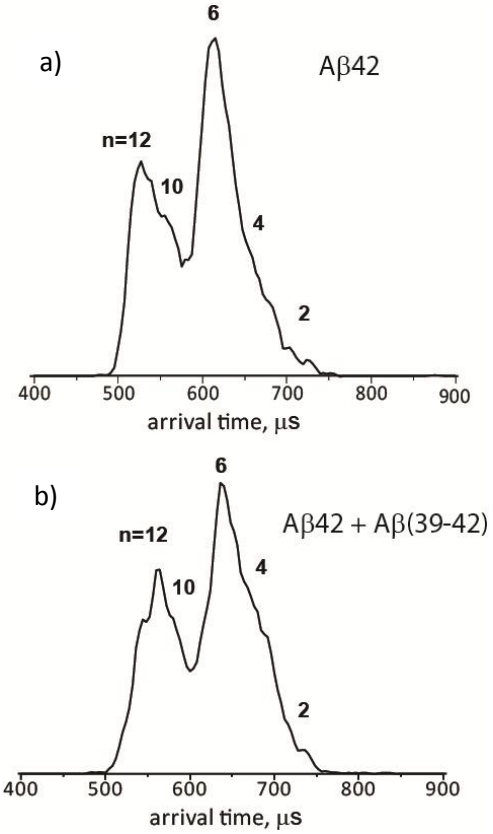

Figure S4 ATD of z/n=-5/2 for n[2Aβ40 + Aβ(39-42)]$^{-5n}$. Features corresponding to the dimer (n=2) and tetramer (n=4) are present, as determined by cross section measurements.

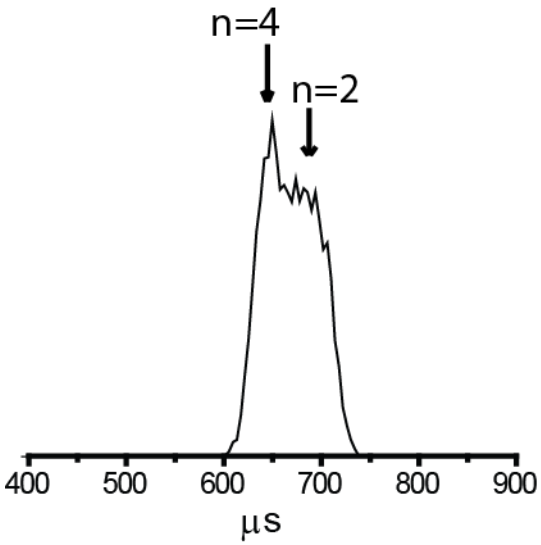

Table S1 Experimental Cross sections of each feature in the z/n= -5/2 ATD of Aβ42 and Aβ40 in solutions in the absence of presence of Aβ(39-42).

Solution	Cross Section (Å^2)				
	n=12	n=10	n=6	n=4	n=2
Aβ42 Blank	4470	3870	2750	2339	1261
Aβ42 + Aβ(39-42)	n/a	n/a	2742	2290	1234
Aβ40 Blank	n/a	n/a	n/a	2120	1260
Aβ40 + Aβ(39-42)	n/a	n/a	n/a	2136	1241

The Aβ:CTF complex

The starting structures of β42, Aβ40, and Aβ(39-42) that were used for the binding simulation are shown in Figure S5. These are the most abundant structures from previous studies, as stated in the methods section of the main text. Validate our choice of force field, we have carried out an additional MD simulation of Aβ42 only using the same protocol as our binding simulations for comparison with the NMR data (Figure S6). The calculated J-coupling data show a moderate agreement with the experimental data, which is comparable to the performance by the OPLS force field, the best one among others (AMBER ff94, ff96, GROMOS) examined by Sgourakis et al(*22*). In addition, strong propensity to form helical structure was not observed. This is consistent with the recent study(*30*) that shows that both AMBER ff03 and ff99SB offer significant improvements in the balance between helix and β-sheet, compared to early versions (ff94, ff96 and ff99). For the binding simulation, four trajectories were run for Aβ(39-42) binding to Aβ42 (Figure S7) and for Aβ(39-42) binding to Aβ40 (Figure S8). For each system, if the number of atom contacts was greater than 20, the system was designated as being in a bound state. If the total number of contacts was less than 20, Aβ(39-42) was considered unbound.

The resulting, bound systems were grouped into different structural families based on the Cα root mean square deviation (RMSD) of the complex (cutoff of 5 Å) using the GROMACS protocol. Representative complexes of Aβ42 and Aβ(39-42) from the most populated structural families (a-f) are shown in Figure S9. Representative complexes of Aβ(39-42) binding to Aβ40 from the most populated structural families (A-F) are shown in Figure S10.

Experimental collision cross sections were measured in IMS experiments for Aβ42 and Aβ40 with one and two CTFs bound (Figure S11; Table S2). The ATD of each species shows two features, similar to the ATD of Aβ with no CTFs bound (also shown in Figure S11). We have previously shown that, in the case of wild-type Aβ40 and Aβ42, these features correspond to a compact gas phase structure and an extended, solution-like structure. Similarly, in each case the feature at shorter arrival times has a cross section that is much smaller than any of the dehydrated structures calculated, suggesting that this feature is, in fact, a compact gas-phase structure. In both the case of the Aβ40:CTF and Aβ42:CTF complex, the cross section of the feature at longer arrival times is in good agreement with the cross sections of the dehydrated,

solution-phase structures (Fig S11). Although we do not have MD-calculated structures for Aβ40 and Aβ42 with two CTFs bound, we see a similar trend of ATDs with two features, suggesting that again, this ATD consist of a compact, gas-phase structure and a more extended, solution-like structure.

Figure S5 The starting structures of Aβ42, Aβ40, and Aβ(39-42), as derived from previous studies. The side-chains of E22, D23 and K28 are shown (blue: positively charged, red: negatively charged). The α-helical, 3-10-helical, β-extended, β-bridged, turn and coiled conformations are colored in purple, blue, yellow, tan, cyan and white. The positively charged N-termini and negatively charged C-termini are indicated by blue and red balls, respectively.

Aβ42

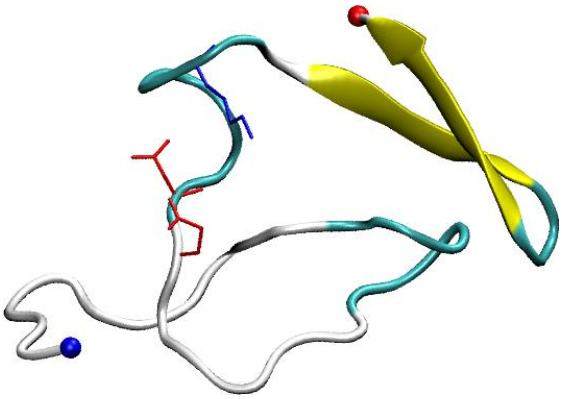

Aβ40

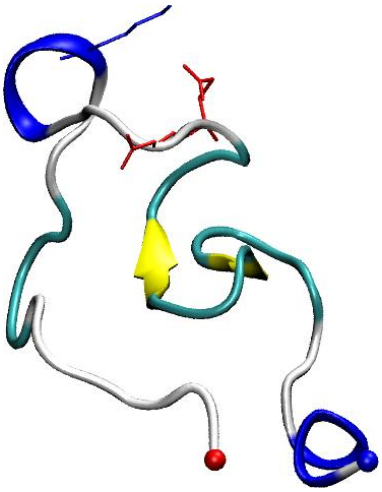

Aβ(39-42)

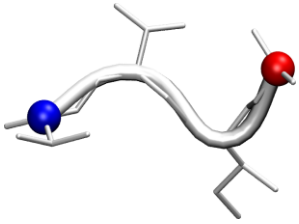

Figure S6 Force field validation. A: J-coupling data ($^3J_{HNH\alpha}$) from the study by *Sgourakis et al* (*22)* B: Secondary structure propensity. The calculation is from the 150 ns MD simulation of Aβ42 alone, using the same protocol as in our binding simulations. The correlation coefficient between the experiment and the simulation data is 0.48, which is slightly better than 0.43 of the simulation using the OPLS force field (*22*). There is no strong helical propensity over the duration of the simulation.

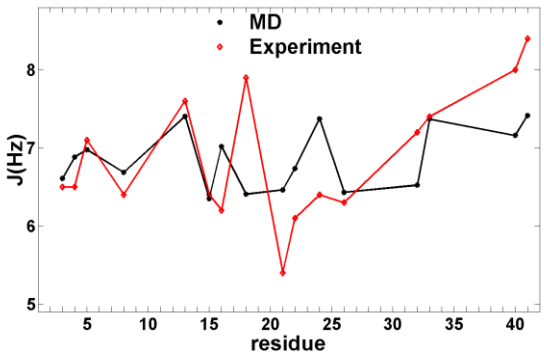

A

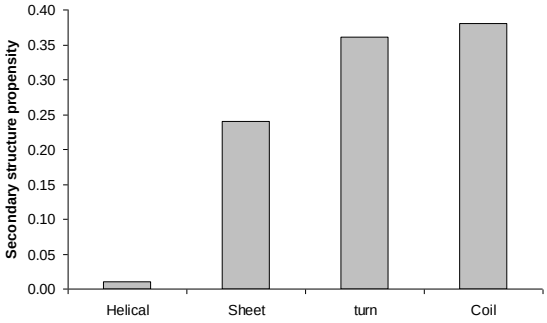

B

Figure S7 Binding of Aβ(39-42) to Aβ42 in each of the 4 trajectories. The distance cutoff for atom contacts between two peptides is set to be 3 Å.

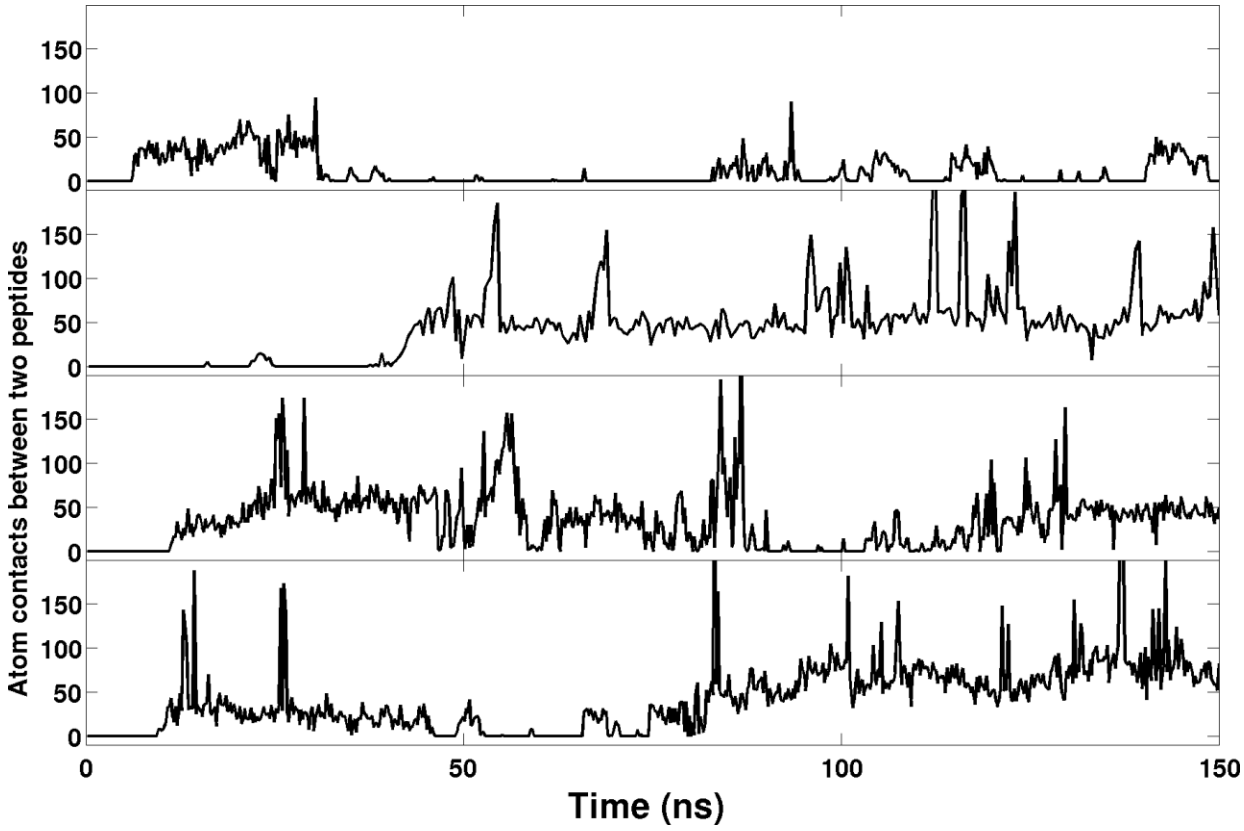

Figure S8 Binding of Aβ(39-42) to Aβ40 in each of the 4 trajectories. The distance cutoff for atom contacts between two peptides is set to be 3 Å.

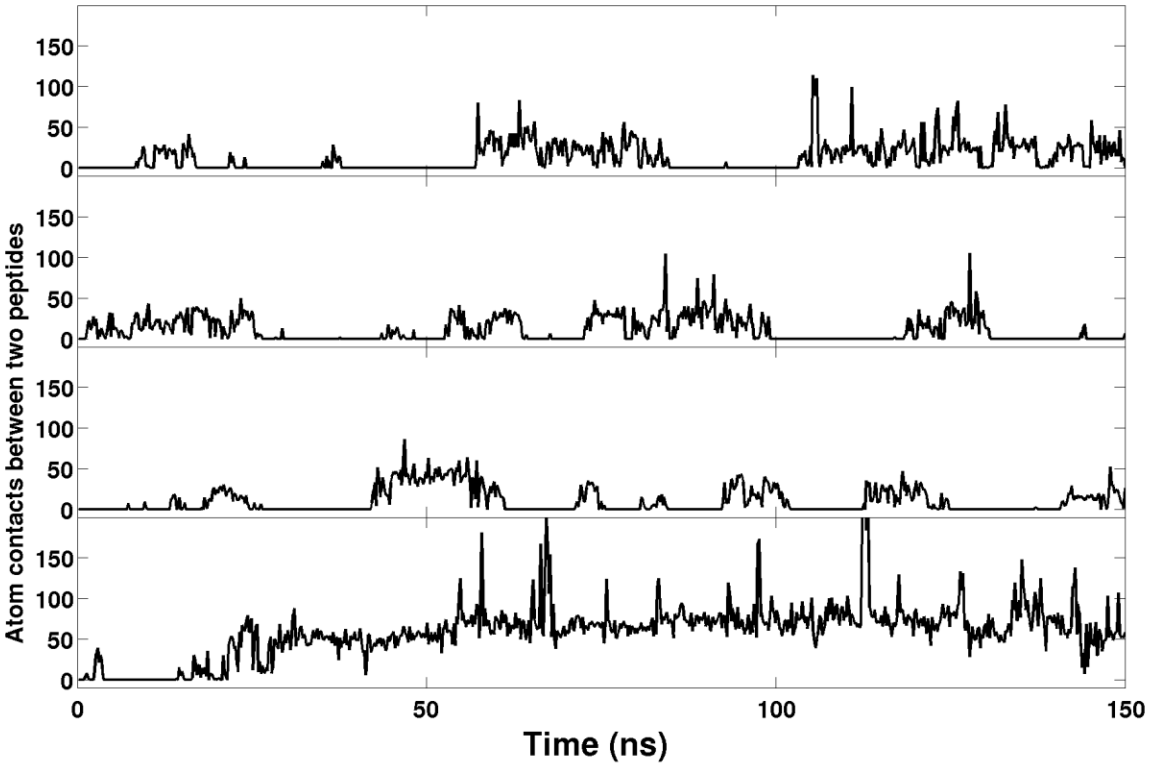

Figure S9 Representative structures of the Aβ(39-42):Aβ42 complexes from the most populated structural families (a-f). Only the side-chains in contact with Aβ(39-42) are shown (blue: positively charged, red: negatively charged and black: hydrophobic). The backbone of Aβ(39-42) is also in black. α-helical, 3-10- helical, β-extended, β-bridged, turn and coiled conformations of Aβ42 are colored in purple, blue, yellow, tan, cyan and white, respectively. The positively charged N-termini and negatively charged C-termini are indicated by blue and red balls respectively. The abundance is noted below each structure.

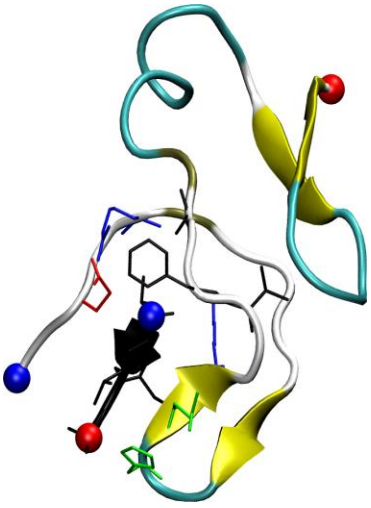

a (29%)

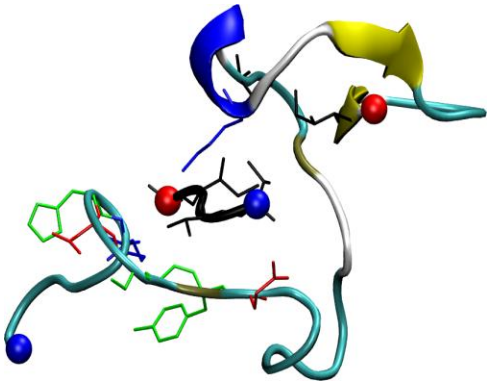

b (15%)

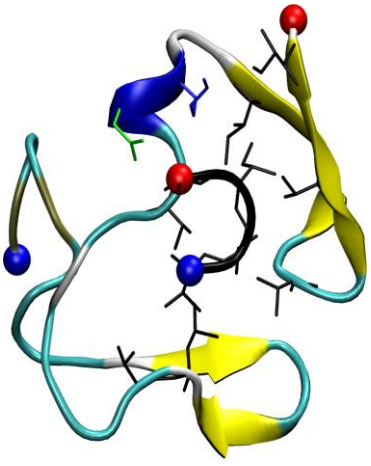

c (13%)

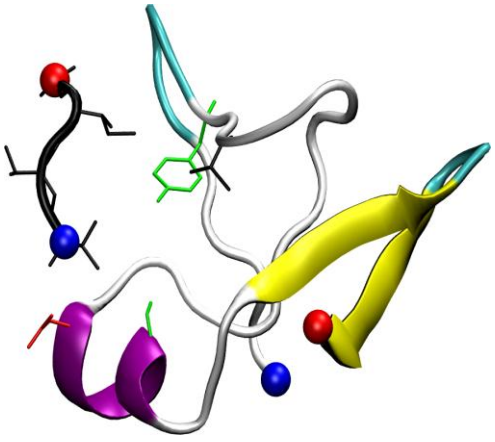

d (9%)

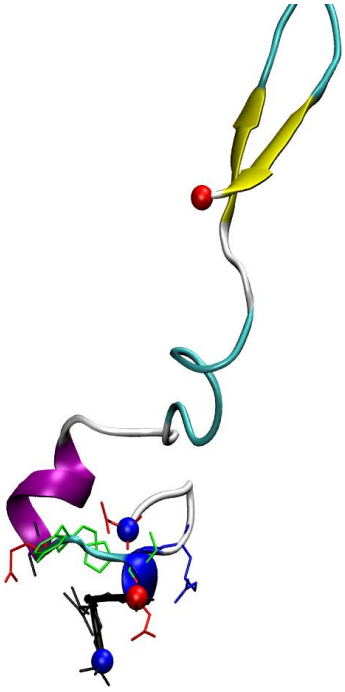

e (8%)

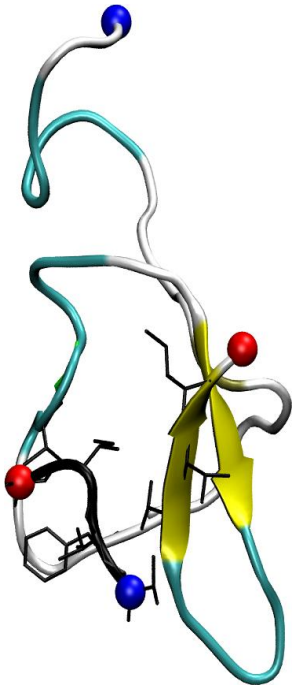

f (5%)

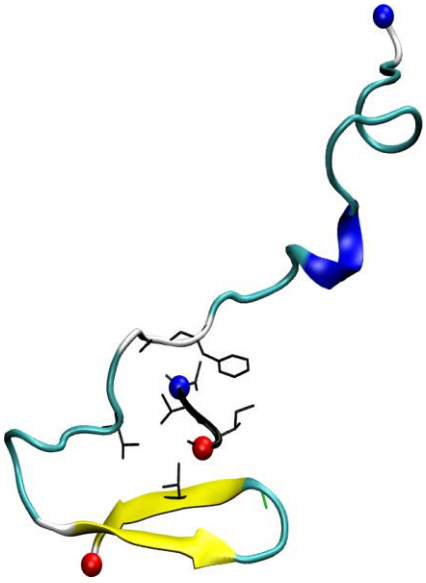

g (4%)

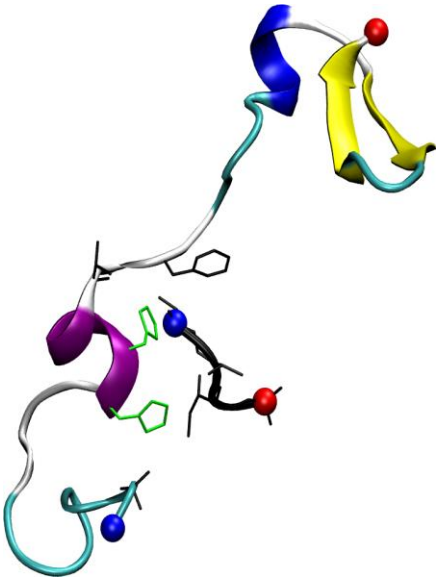

h (2%)

Figure S10 Representative structures of the Aβ42:Aβ(39-42) complex from the most populated structural families(A-F). Only the side-chains in contact with Aβ(39-42) are shown (blue: positively charged, red: negatively charged and black: hydrophobic). The backbone of Aβ(39-42) is also shown in black. The α-helical, 3-10-helical, β-extended, β-bridged, turn and coiled conformations of Aβ42 are shown in purple, blue, yellow, tan, cyan and white, respectively. The positively charged N-termini and negatively charged C-termini are indicated by blue and red balls, respectively. The abundance is noted below each structure.

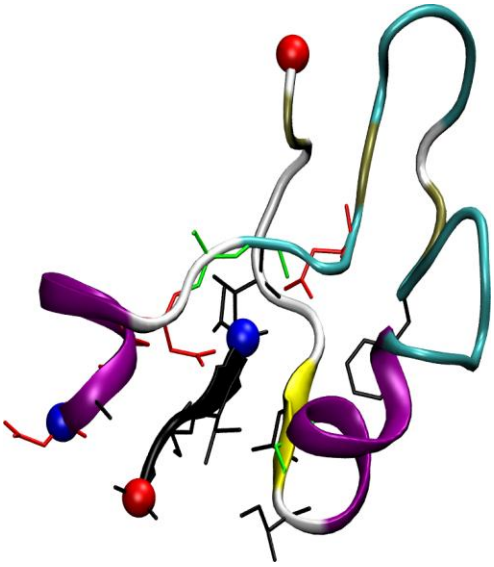

A (38%)

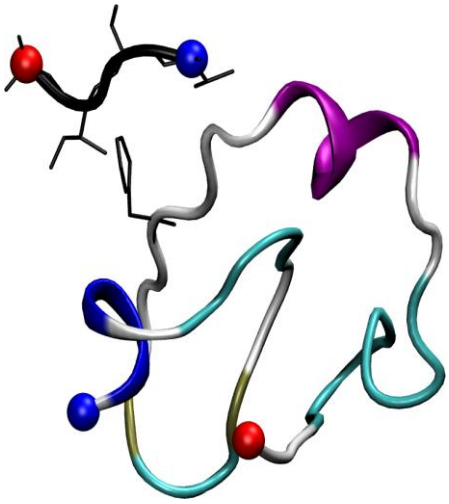

B (18%)

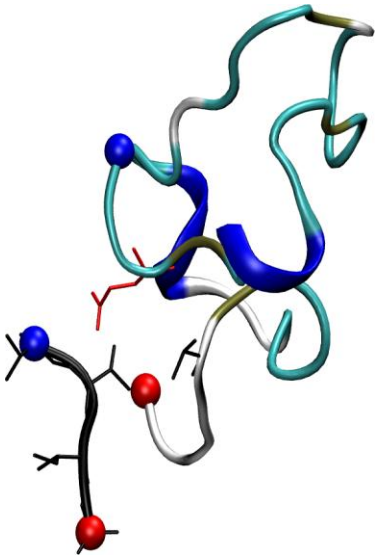

C (13%)

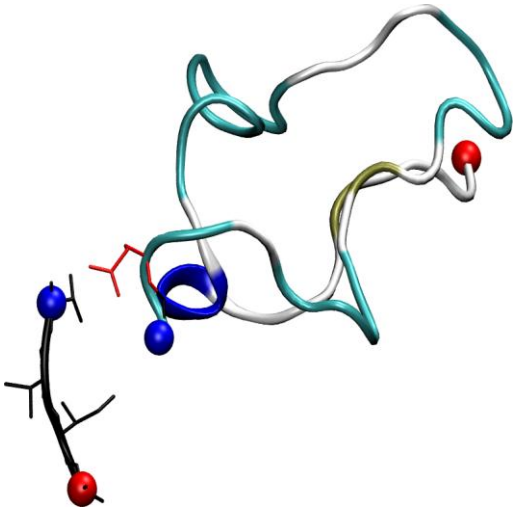

D(11%)

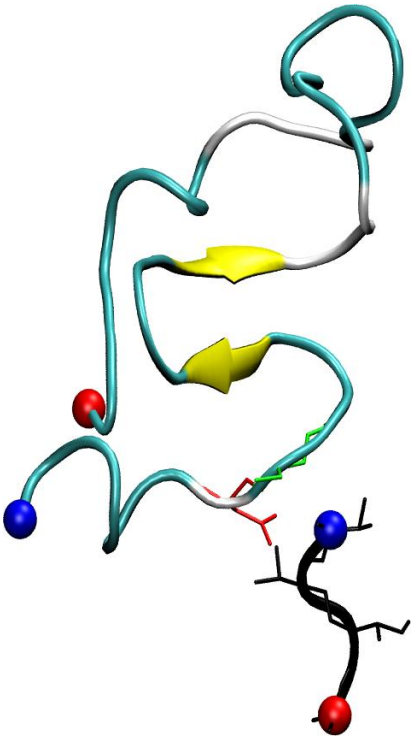

E (11%)

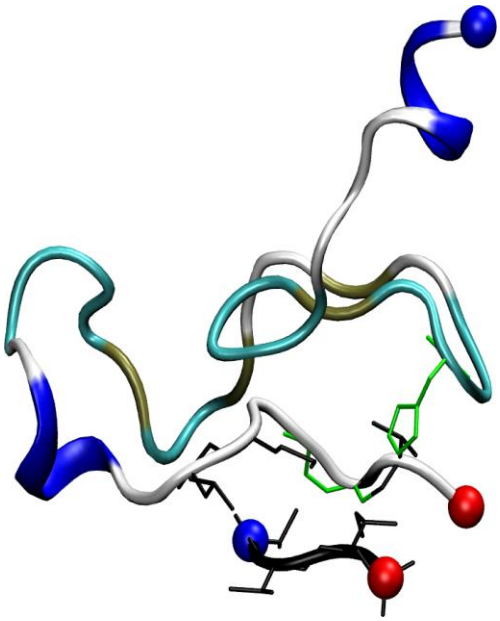

F (3%)

Figure S11 ATDs of z/n=-3 of Aβ, Aβ bound with one Aβ(39-42) peptide, and Aβ bound with two Aβ(39-42) peptides (Above: Aβ, Below: Aβ).

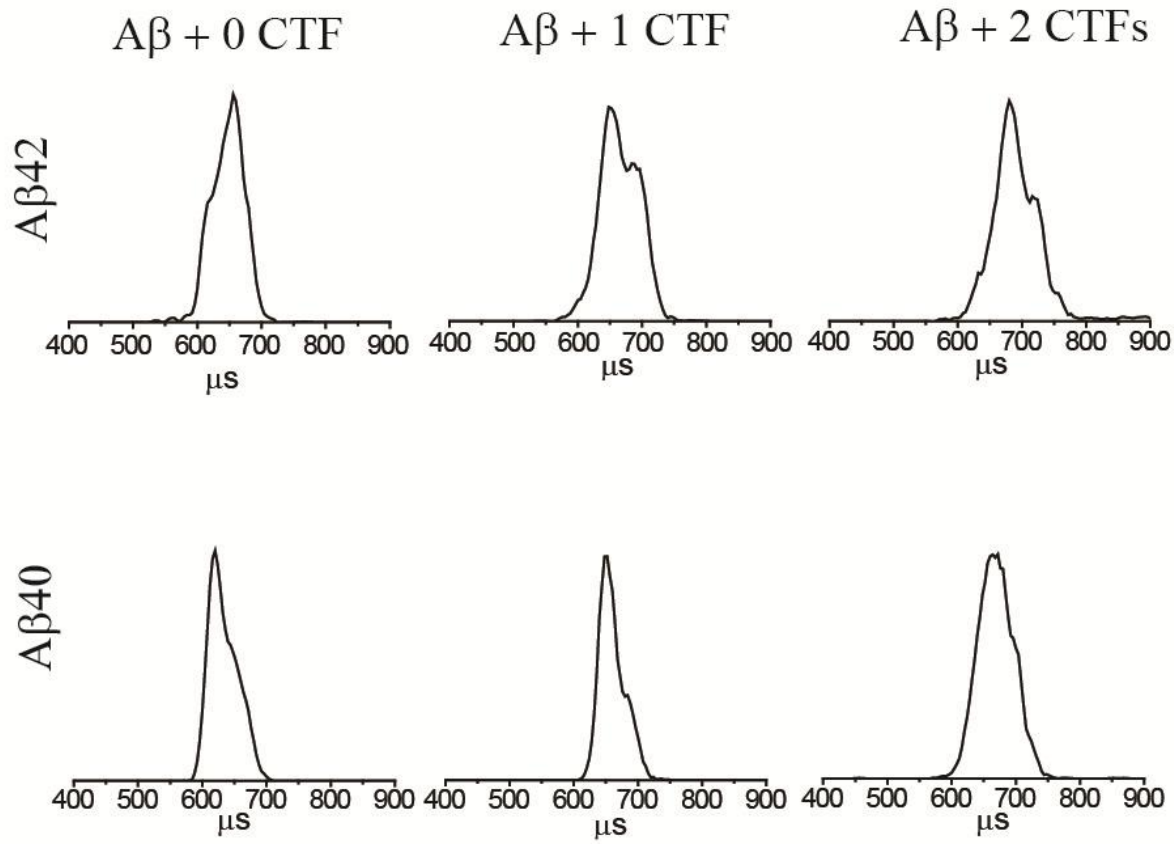

Table S2 Experimental Cross sections of the z/n=-3 charge state of Aβ42 and Aβ40 with and without Aβ(39-42). Two features were present for every ATD and the cross section of both features is provided in each case. Experimental error is included for each measurement, as well.

	Cross Section ($Å^2$)					
	0 CTF		1 CTF		2 CTF	
Aβ42	636 ± 7	693 ± 5	698 ± 11	729 ± 12	751 ± 13	780 ± 12
Aβ40	617 ± 9	679 ± 12	650 ± 5	689 ± 3	651 ± 12	701 ± 10